Electronic Supplementary Material (ESI) for Environmental Science: Nano.

Supplementary Information

Nanoparticle Aggregation in a Freshwater River: The Role of Engineered Surface Coatings

Mark C. Surette and Jeffrey A. Nason

School of Chemical, Biological and Environmental Engineering

Oregon State University, 116 Johnson Hall, Corvallis, Oregon 97331, United States

22 Pages
14 Tables
6 Figures

Intensity- vs. Number-Weighted Hydrodynamic Diameter

Inspection of the multi-modal size distribution (MSD) generated during the initial sizing of the model engineered nanoparticles (ENPs) indicates the presence of few, small aggregates and/or particle contaminants in the samples. As noted in Table S1, intensity-weighted hydrodynamic diameter (D_h) reported by the manufacturer was generally consistent with the 'initial peak' calculated by the MSD analysis (i.e., the peak expected to be representative of the model ENPs). Likewise, the number-weighted D_h measured for the entire sample (also reported in Table S1) was similar to the intensity-weighted, 'initial peak' D_h. Overall, these various measurements indicate that the primary particles were in the range of ≈20 – 30 nm, which is within expectations given the engineered surface coatings possessed by the model ENPs.

Table S1. Manufacturer reported intensity-weighted D_h and 'as-received' intensity- and number-weighted D_h of model ENPs.

Surface Coating	Intensity-Weighted D_h (nm)		Number-Weighted D_h (nm)
	Manufacturer-Reported	MSD Initial Peak	
2 kDa PEG	N/A	20.3 ± 10.4	19.8 ± 10.2
3 kDa PEG-COOH	35	29.1 ± 12.4	22.5 ± 13.8
3 kDa PEG-Amine	31	32.0 ± 7.7	31.0 ± 7.4
25 kDa bPEI	47.6	15.1 ± 42.6	14.1 ± 40.7
Citrate	18	20.4 ± 3.2	8.0 ± 9.2

Error bars indicate ± 95% confidence interval; (PEG) n = 4; (PEG-COOH) n = 7; (PEG-Amine) n = 7; (bPEI) n = 2; (Cit) n = 4.

Electrophoretic Mobility/Zeta Potential of Model Engineered Nanoparticles

The electrophoretic mobility (EPM) of the model ENPs were measured in pH-adjusted 1 mM KCl at 10 mg Au/L (Table S2) according to the procedures detailed in Surette and Nason (2016).

Table S2. Electrophoretic mobility (EPM) of model ENPs.

Surface Coating	Electrophoretic Mobility ([µm/S] / [V/cm])
2 kDa PEG	-1.22 ± 0.2 (pH 6.8 ± 0.03)
3 kDa PEG-COOH	-1.23 ± 0.2 (pH 7.1 ± 0.1)
3 kDa PEG-Amine	-0.71 ± 0.1 (pH 7.0 ± 0.1)
25 kDa bPEI	1.20 ± 0.1 (pH 6.8 ± 0.1)
Citrate	-2.26 ± 0.2 (pH 7.4 ± 0.1)

Error bars indicate ± 95% confidence interval (n = 15).

The measured EPM (μ_E) were then converted to zeta potential (ζ) according to Henry (1931) with the correction $f_1(\kappa a)$ applied according to Ohshima (1994), resulting in the following equation:

$$\zeta = \frac{3\mu_E\eta}{2\epsilon_w f_1(\kappa a)} = \frac{3\mu_E\eta}{2\epsilon_w\left(1+\frac{1}{2\left[1+\frac{\delta}{\kappa a}\right]^3}\right)} \quad (1)$$

Where:

$$\delta = \frac{2.5}{1+2e^{-\kappa a}} \quad (2)$$

The definition of the variables in Equations 1 and 2, along with their corresponding values, are shown in Table S3. The calculated value of ζ for each model ENP is shown in the main text (Table 1).

Table S3. Inputs used to calculate ζ from μ_E.

Input	Value	Source
Permittivity in Water (ϵ_w)	$6.95x10^{-10}$ C^2/J-m	Known – H_2O
Medium Dynamic Viscosity (η)	1 $x10^{-3}$ N-s/m^2	Known – H_2O
Ohshima Fitting Parameter (δ)	1.2 – 1.3	Hunter (2001)
Inverse Debye Length (κ)	0.104 nm^{-1}	Calculated per Benjamin & Lawler (2013)
Particle Radius (a)	5.25 – 7.5 nm	Measured (Table 1)

All values at 25 ºC.

River Water Characteristics

Samples of the Willamette River water (WRW) obtained on June 30, 2017 were characterized according to the methods described in the American Water Works Association (AWWA) *Standard Methods for the Examination of Water and Wastewater, 22nd Edition* (American Public Health Association, 2012). All analyses were performed in triplicate and were completed within 21-days of sample collection according to their method-specific holding times. All samples that were collected for analysis of the dissolved fraction were filtered within 3 hours after collection. Samples that were collected for total metals analysis were acid-preserved immediately upon collection. Samples that were collected for dissolved metals analysis were first filtered (using pre-washed filters) and then acid-preserved immediately following filtration. A summary of the results and the associated *Standard Methods* are provided in Table S4.

The particle size distribution (PSD) of the background natural colloids was determined via Coulter Counter according to Method 2560-B. Three separate samples were analyzed in triplicate (n = 9), with all runs performed at 5% v/v raw WRW dispersed in 0.45 µm filtered ISOTON II® (Beckman Coulter) as the background electrolyte solution. The Coulter Counter was operated in total-count mode (≥ 10,000 total counts) using a 30 µm aperture with the current at -400 µA, flow at 3.5 µL/s, gain at 8, and resistivity at 54.4 kΩ. The detection range was between 0.746 – 30 µm (lower- and upper-limits, respectively). The PSD (Figure S1) was generated by averaging the number of particles within each size 'bin' across the replicate measurements.

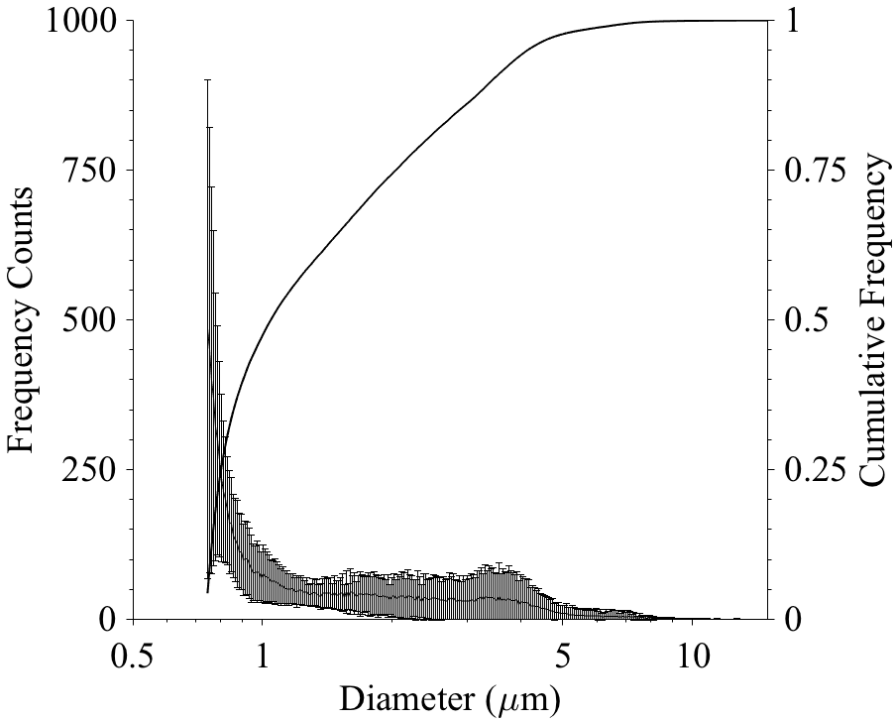

Figure S1: Particle size distribution of natural colloids in raw WRW measured via Coulter Counter. Error bars indicate ± 95% confidence interval (n = 9).

Table S4. Summary of Willamette River water quality parameters/characteristics.

Parameter	Value	Unit	Method
Total Organic Carbon (TOC)	0.80 ± 0.0	mg C/L	Method 5310-B
Dissolved Organic Carbon (DOC)	0.83 ± 0.1	mg C/L	
Dissolved Cations:			Method 3125
Ca^{2+}	4.85 ± 0.43	mg/L	
Mg^{2+}	1.58 ± 0.38	mg/L	
Na^{+}	4.04 ± 0.13	mg/L	
K^{+}	0.63 ± 0.23	mg/L	
Fe^{3+}	N/D	mg/L	
Dissolved Anions:			Method 4110-C
F^{-}	N/D	mg/L	
Cl^{-}	1.83 ± 0.04	mg/L	
NO_2^{-}	N/D	mg/L	
NO_3^{-}	0.51 ± 0.0	mg/L	
SO_4^{2-}	2.71 ± 0.01	mg/L	
pH	7.9 ± 0.10		Probe Measurement
Total Suspended Solids (TSS)	3.9 ± 0.4	mg/L	Method 2540-D
Total Alkalinity	25.0	mg/L as $CaCO_3$	Method 2320
Total Hardness	18.6	mg/L as $CaCO_3$	Method 2340-B

Error bars indicate ± one standard deviation on the mean (n = 3).

Filter Washing Procedure

To prepare the filtered WRW, the procedures recommended by Karanfil et al. (2003) were followed. Prior to use, the filters were washed with approximately 1L (0.45 µm PES filters) or 0.5 L (0.02 µm syringe filters) of 18.2 MΩ-cm distilled, deionized (DDI) water (EGLA Purelab). After washing and upon initiation of sample filtration, the first 50 mL of the filtrate was discarded. This process was repeated at each sequential filtration stage (i.e., decreasing pore size).

To verify whether organics were leached from the filter material, the organic carbon (OC) concentration was measured at three points along the sequential filtration steps. The total organic carbon (TOC) was measured for the raw WRW to provide a baseline OC concentration. Samples were then collected and analyzed following 0.45 µm filtration (operationally defined as DOC) and again following the 0.02 µm filtration.

The results, summarized in Table S5, show that there was no statistically significant difference in the measured OC concentration following each filtration step (unfiltered to 0.45 µm: paired *t*-test(1) = 4.25, $p = 0.15$; 0.45 µm to 0.02 µm: paired *t*-test(1), = 2.32 $p = 0.26$; unfiltered to 0.02 µm: paired *t*-test(2) = 4.39, $p = 0.05$).

Table S5. Measured organic carbon concentration following each filtration step.

Parameter	Value	
Total Organic Carbon (TOC)	0.80 ± 0.01	mg C/L
Dissolved Organic Carbon – 0.45 µm Filtration	0.83 ± 0.05	mg C/L
Dissolved Organic Carbon – 0.02 µm Filtration	0.95 ± 0.15	mg C/L

Error bars indicate ± 95% confidence interval ($n = 2 – 3$).

Calculation of Average Shear Rate

The average shear-rate was calculated according to the equations provided in Croughan et al. (1987), which are summarized below, and the inputs provided in Table S6.

$$G = \frac{112.8 N r_i^{1.8} \left(r_t^{0.2} - r_i^{0.2}\right)(r_c/r_i)^{1.8}}{r_t^2 - r_i^2} \quad (3)$$

$$\frac{r_c}{r_i} = \frac{Re}{(1000 + 1.6Re)} \quad (4)$$

$$Re = \frac{N D_i^2 \rho}{\mu} \quad (5)$$

Table S6. Inputs used to calculate the average shear rate (*G*).

Parameter	Value	Units
Impeller Speed (*N*)	400	rpm
Impeller Radius (r_i)	11	mm
Impeller Diameter (D_i)	22	mm
Mixing Vessel Radius (r_t)	17.5	mm
Radius of Forced Vortex Zone (r_c)	5.9	mm
Medium Dynamic Viscosity (μ)	0.0089	g/cm-s
Medium Density (ρ)	0.997	g/cm^3

Centrifugation Testing – Removal Natural Colloids

The intent of this test was to optimize the removal of the background natural colloids (NCs) within the river water sample (as well as any attached model ENPs, when present), while minimizing the removal of any unaggregated model ENPs (tested separately; details below).

1. Three 15-mL polypropylene centrifugation vials (Falcon™, BD Biosciences) were each filled with 6 mL of raw WRW.
2. The triplicate samples were then centrifuged at 3,500 rpm (≈ 2,200 g RCF) for various durations—2, 5, and 10 minutes.
3. After centrifugation, 3 mL of the supernatant was removed and analyzed via dynamic light scattering (DLS) via 3 measurement runs, each 3 minutes long to measure the post-centrifugation *z*-average hydrodynamic diameter (D_h).

Using the medium density (ρ = 0.998 g/cm^3), viscosity (μ = 0.01 g/cm-s), and an assumed value for the density of the NCs (ρ_{NC} = 2.65 g/cm^3) in combination with the experimental conditions (i.e., centrifugation speed/duration), a theoretical particle size threshold was established. For the given system at 3,500 rpm (≈2,200*g* RCF) and 5 minutes centrifugation, NCs with $D_h \geq \approx$300 nm should be removed. The results of the post-centrifugation D_h measurements obtained via DLS, provided in Table S7, closely match the predicted particle size threshold.

Table S7. Measurement of D_h of the background natural colloids following centrifugation.

Duration of Centrifugation	Post-Centrifugation (D_h) (nm)
2 Minutes	313.5 ± 17.2
5 Minutes	303.3 ± 28.3
10 Minutes	252.9 ± 16.9

Error bars indicate ± one standard deviation on the mean (n = 3).

The gauge the extent of NC removal via centrifugation, the turbidity of the unaltered WRW was measured before and after centrifugation (at 3,500 rpm for 2 minutes). The results, shown in Table S8, indicate the turbidity decreased by ≈66%, demonstrating that a fraction of the background NCs remained in suspension following centrifugation.

Table S8. Pre- and post-centrifugation turbidity of unaltered WRW.

Sample	Turbidity (NTU)
Pre-Centrifugation	3.41 ± 0.69
Post-Centrifugation	1.17 ± 0.25

Error bars indicate ± one standard deviation on the mean (n = 3).

To extend this analysis further, we applied the Random Sequential Adsorption (RSA) model detailed by Sadowska et al. (2014) to determine if very small NCs (i.e. d_{NC} < 300 nm) that had heteroaggregated with the model ENPs could remain in suspension following centrifugation. To accomplish this, we calculated the maximum fractional surface coverage (θ_{max}) of a model NC that could be "occupied" by model ENPs. From this, we estimated the total number of model ENPs that could attach to a single model NC and estimated the spherical-equivalent density and size of the ENP-NC heteroaggregate. We then determined whether such an ENP-NC heteroaggregate would be removed via centrifugation at the speed and duration used in our experimental method (i.e., 3,500 rpm for 2 minutes). There are a number of assumptions that are required to perform this analysis. For the model NC, we assume it is a monodisperse spherical collector with the density of SiO_2 (ρ = 2.65 g/cm^3). Furthermore, we assume that the model ENPs are present on the model NC at θ_{max}. Although θ_{max} is calculated by incorporating electrostatic interactions between adjacent model ENPs, it ignores steric interactions that are known to be occurring.

The results indicate that a model NC covered with model ENPs to the extent estimated by θ_{max} would remain in suspension following centrifugation up to $d_{NC} \leq$ 280 nm. This cut-off is slightly lower than that estimated previously. While confirming that this phenomena is possible within our experimental system, the impacts on our experimental results are much harder to estimate. Furthermore, this analysis represents a worst-case scenario by ignoring the presence of large NCs (i.e., d_{NC} > ≈300 nm), assuming that homoaggregation does not occur (i.e., α_{homo} = 0), ignoring particle transport processes (β), and assuming that α_{hetero} = 1.0.

Centrifugation Testing – Removal of AuNPs

The intent of this test was to assess and quantify the losses of the model ENPs that may be attributed to the centrifugation process. Based upon previous testing, each model ENP was known to be stable when dispersed in 0.02 µm filtered 18.2 MΩ-cm distilled, deionized water (DDI; EGLA Purelab). Thus, following dispersion into DDI and following centrifugation, any difference in the AuNP concentration before and after centrifugation could be quantified and attributed to loss during the centrifugation process. A preliminary test was first performed at 3,500 rpm (≈ 2,200 *g* RCF) for 5 minutes using the following procedure.

1. Five 15-mL polypropylene centrifugation vials (Falcon™, BD Biosciences) were each filled with 7.2 mL of 0.02 µm filtered DDI and well-mixed with 0.8 mL of a given model ENP type (C_{NP} = 5 mg/L). One replicate for each model ENP type was prepared.
2. Prior to centrifugation, 3 mL was removed from each sample, transferred to a quartz cuvette, and analyzed via UV-Vis at λ = 520 nm to measure the pre-centrifugation concentration.
3. The remaining 5 mL was centrifuged at 3,500 rpm (≈ 2,200 g RCF) for 5 minutes.
4. After centrifugation, the top 3 mL was removed, transferred to a quartz cuvette, and analyzed via UV-Vis at λ = 520 nm to measure the post-centrifugation absorbance.

The results of the preliminary test are provided in Table S9. Based upon the results, it was decided that a shorter duration centrifugation time should be tested to see if the percent loss could be reduced. The same approach detailed above was followed, except that triplicate samples of each model ENP were prepared and were centrifuged at 3,500 rpm (≈ 2,200 *g* RCF) for 2 minutes.

Table S9. Measurement of AuNP concentration before and after centrifugation (5-minute duration).

Model ENP	Pre-Centrifugation C_{NP} (mg/L)	Post-Centrifugation C_{NP} (mg/L)	Percent Change
bPEI	4.81	4.58	-4.7%
Cit	4.37	3.12	-28.6%
PEG-COOH	4.11	2.81	-31.7%
PEG-Amine	5.05	4.63	-8.2%
PEG	4.98	1.66	-66.7%

The results for the additional testing, shown in Table S10, indicate that for all model ENPs tested, the losses due to centrifugation were reduced when centrifuging for 2 minutes versus 5 minutes (Table S9). The combination of 3,500 rpm (≈ 2,200*g* RCF) for 2 minutes was selected for use in the batch experiments, based upon these results and the results indicating only a minimal decrease in the size of NCs removed (Table S7) using the shorter centrifugation duration.

Even when using the shorter centrifugation duration, there were still measurable losses for the Cit-, PEG-COOH-, and PEG-AuNPs. To account for this, the AuNP concentrations measured via ICP-OES during the batch experiments were increased by multiplying the 'as-measured/undiluted' Au concentration by a correction factor (Cit: 1.085; PEG-COOH: 1.206; PEG: 1.190).

Table S10. Measurement of AuNP concentration before and after centrifugation (2-minute duration).

Model ENP	Pre-Centrifugation C_{NP} (mg/L) [a]	Post-Centrifugation C_{NP} (mg/L) [a]	Percent Change
bPEI	4.8 ± 0.1	4.9 ± 0.1	+2.3%
Cit	3.9 ± 0.2	3.5 ± 0.2	-8.5%
PEG-COOH	3.8 ± 0.1	3.0 ± 0.1	-20.6%
PEG-Amine	5.0 ± 0.1	5.0 ± 0.1	<1.0%
PEG	4.8 ± 0.1	3.9 ± 0.1	-19.0%

Error bars indicate ± one standard deviation on the mean (n = 3).

Vial Interactions – Loss of AuNPs to Centrifugation Vials

The results from the centrifugation testing (Table S10) indicated that significant losses were still observed for the PEG-COOH- and PEG-AuNPs (-20.6% and -19.0%, respectively), even at the shorter centrifugation duration. Based upon this, it was decided to further explore these losses to determine if they were associated with interactions between the model ENPs and the centrifugation vials. The following procedure was applied:

1. Six 15-mL polypropylene centrifugation vials (Falcon™, BD Biosciences) were each filled with 8.1 mL of 0.02 µm filtered DDI and well-mixed with 0.9 mL of a given model ENP type (C_{NP} = 5 mg/L). Triplicate samples for PEG-COOH- and PEG-AuNPs were prepared.
2. Immediately upon combination, 3 mL was removed from each sample, transferred to a quartz cuvette, and analyzed via UV-Vis at λ = 520 nm to measure the absorbance.
3. Additional samples were removed and analyzed at t = 10 and 30 minutes from each replicate and analyzed according to the same procedures.

The results, shown in Figure S2, indicate that no statistically significant difference in the absorbance occurred over the 30-minute period (PEG-COOH: paired *t*-test(2) = 0.74 *p* = 0.54; PEG: paired *t*-test(2) = 3.01 *p* = 0.09). These results show that the losses noted during the centrifugation testing (Table S10) were associated with the centrifugation process.

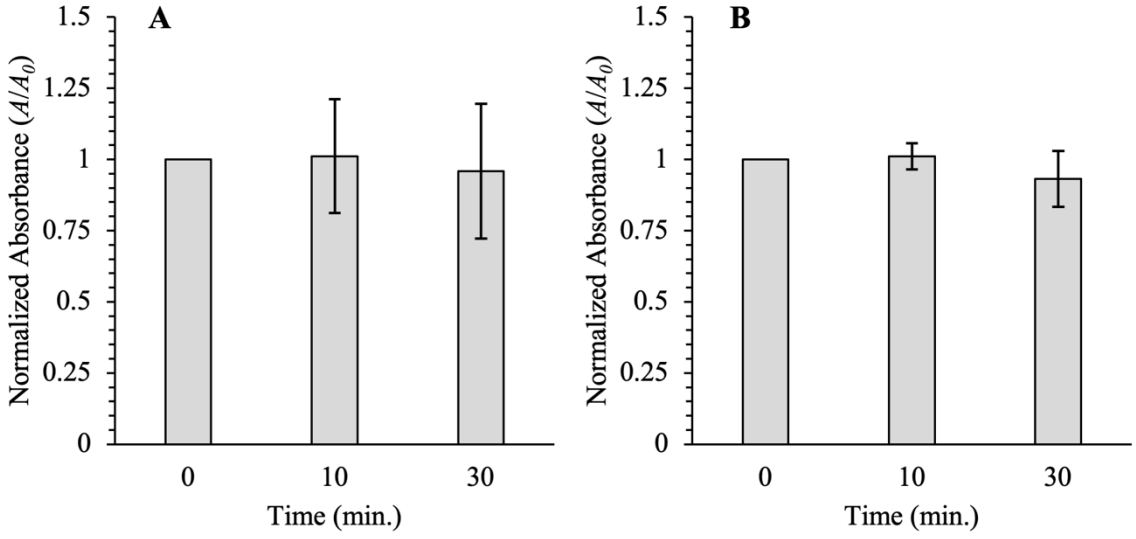

Figure S2: Normalized absorbance (A/A_0) over time for (**a**) PEG-COOH- and (**b**) PEG-AuNPs. Error bars indicate ± 95% confidence interval (*n* = 3).

Digestion Technique

Once all sample aliquots were generated for a given batch (n = 42 per batch), each aliquot was acid-digested according to the following procedure:

1. Each aliquot, contained within a perfluoroalkoxy alkane (PFA) vial, was placed on a heat plate, uncapped, and heated to 200 ^{o}C to evaporate off the water.
2. Once a small amount of residue remained (≈25 µL), 2.5 mL of freshly-prepared *aqua regia* (3:1 ultrapure HCl:HNO_3) was added to each PFA vial and heated at 200 ^{o}C to evaporate off the *aqua regia*.
3. When a small drop of aqua regia/residue remained, the PFA vials were removed from the heat plate and 1 mL of 3+1 *aqua regia* (3:1 DDI:*aqua regia*) was added to each PFA vial. The vials were then allowed to cool to room temperature.
4. After cooling to room temperature, 1 mL from each PFA vial was transferred, via calibrated pipette, to a 50-mL polypropylene centrifuge tube (Falcon™, BD Biosciences) containing 10 mL of DDI. After this first transfer, a series of five additional wash/transfer steps were performed as follows: 1 mL of 3+1 *aqua regia* (3:1 DDI:*aqua regia*) was added to each PFA vial, being careful to rinse down the sidewalls of the vials, and then 1 mL from each PFA vial was transferred, via calibrated pipette, to their respective 50-mL polypropylene centrifuge tube.
5. The total, final volume of each polypropylene vial was recorded and the tubes were stored at 4 ^{o}C until ready for analysis via ICP-OES.

Digestion Technique – Spike/Recovery Testing

To verify that the digestion technique resulted in adequate recovery (i.e., >90%) of the model ENPs upon their introduction to the river water, a spike/recovery test was performed. The intent of the spike/recovery test was to mimic the experimental procedure used in the batch experiments but generate a 'worst-case' scenario where no model ENPs are removed via centrifugation following interactions with the natural colloids. To do this, the model ENPs were spiked into the samples following the centrifugation step.

1. Six 15-mL polypropylene centrifugation vials (Falcon™, BD Biosciences) were each filled with 5 mL of raw WRW and centrifuged at 3,500 rpm (≈ 2,200 *g* RCF) for 2 minutes.
2. Immediately following sample centrifugation, a 4-mL sample of the supernatant was collected from each 15-mL vial and transferred to a separate 7-mL PFA vial. Each sample was preserved via addition of 10 µL of concentrated (70% w/w) ultra-pure HNO_3.
3. Two sets of samples, prepared in triplicate, were created as follows:

a. Three of the PFA vials were each spiked PEG-Amine-AuNPs to C_{NP} = 500 µg/L by removing and discarding 0.04 mL of the preserved river water and then replacing this volume with 0.04 mL of the model ENP.

b. The remaining three PFA vials were designated as a background sample to measure the Au concentration within the WRW.

4. All six PFA vials were then acid digested according to the procedure outlined above and analyzed via ICP-OES.

5. Following analysis, the percent recovery of each vial spiked with AuNPs was calculated, accounting for the Au mass present within the WRW.

As was expected, the background Au concentration within the WRW was below the analytical detection limit (< 2 µg/L). Therefore, the Au concentration measured in the samples collected during the control testing, as well as the batch experiments, can be solely attributed to the model ENPs introduced into the system. The results for the sample spiked with the AuNPs, summarized in Table S11, indicate good recovery was obtained (103% ± 11%). Thus, the digestion technique was considered adequate to digest the model ENPs within the samples collected during the batch experiments.

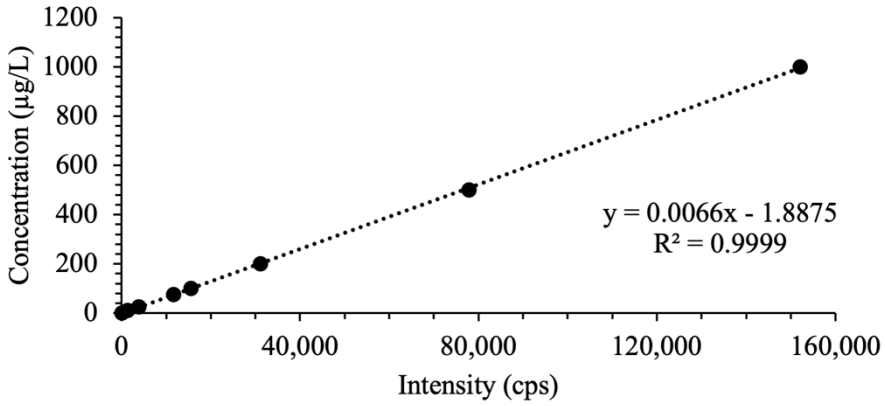

Figure S3: Standard curve generated during spike/recovery testing.

Table S11. Measured AuNP concentration and percent recovery.

Sample	Undiluted Au Concentration (µg/L)	Percent Recovery
Spiked #1	573.13	114.6%
Spiked #2	473.09	94.6%
Spiked #3	495.30	99.1%
Average ± S.D.	513.84 ± 52.53	103% ± 11%

Synthetic Willamette River Water

The synthetic WRW was made by dissolving the salts listed in Table S12 into 1 L of 18.2 MΩ-cm distilled, deionized water (DDI; EGLA Purelab). Upon mixing, the synthetic WRW was adjusted to pH 7.69 and stored at 4 ºC in Nalgene® containers. Prior to use, the synthetic WRW was filtered through a 0.02 µm syringe filter (Anotop®, Whatman). After 24-hours following preparation, the pH of the synthetic WRW was measured again and found to have stabilized at pH 7.48.

Table S12. Composition of synthetic Willamette River water.

Compound	**Mass Added to 1 L (mg)**	**Final Concentration (mM)**
$MgCl_2 \cdot 6H_2O$	6.7	0.033
$CaCO_3$	13.1	0.131
$MgSO_4$	3.6	0.030
KNO_3	0.8	0.0079

Time-Resolved Dynamic Light Scattering (TR-DLS) Measurements

The results of duplicate TR-DLS measurements for each model ENP are shown in Figure S4. Initial aggregation rates ($dD_h/dt|_{t\rightarrow 0}$) were calculated from the TR-DLS data according to the method presented by Chen et al. (2010). Briefly, the initial aggregation rate was calculated from the slope of a linear regression fitted to the data from $D_{h,initial}$ to $1.3D_{h,initial}$, encompassing the region dominated by doublet formation. The slope calculated via the linear regression was then evaluated to determine if it was statistically different than zero (Students *t*-test, $\alpha = 0.05$).

For the PEG- and PEG-COOH-AuNPs, the initial aggregation rates were not statistically different than zero (PEG: *t*-test(50) = -0.80, $p = 0.43$ and *t*-test(106) = -1.13, $p = 0.26$; PEG-COOH: *t*-test(115) = 1.65, $p = 0.10$ and *t*-test(54) = 0.05, $p = 0.96$), thus demonstrating that the PEG- and PEG-COOH-AuNPs were colloidally stable during the TR-DLS measurement period.

For the PEG-Amine and bPEI-AuNPs, there was a near-instantaneous increase in D_h such that the linear regression would be fit to only two data points. As such, an alternative method was used to calculate $dD_h/dt|_{t\rightarrow 0}$ where the $1.3D_{h,initial}$ criterion was adjusted such that the first data-point after $D_{h,initial}$ was used in-lieu of $D_{h,initial}$ to define the region that was regressed (i.e., $D_{h,initial+1}$ to $1.3D_{h,initial+1}$ instead of $D_{h,initial}$ to $1.3D_{h,initial}$). While the results for the PEG-Amine-AuNPs were both statistically different than zero (*t*-test(9) = 7.29, $p \ll 0.001$ and *t*-test(9) = 5.98, $p \ll 0.001$), only one of the linear regression slopes for the bPEI-AuNPs was statistically significant (*t*-test(3) = 2.38, $p = 0.14$ and *t*-test(2) = 14.84, $p = 0.04$). This is likely due to the limited amount of data included in the regression and the resulting sensitivity to variability between the D_h measured at each time point. Since the TR-DLS measurement profiles for the bPEI-AuNPs, as well as the PEG-Amine-AuNPs, clearly demonstrate that these model ENPs aggregated, both of the calculated $dD_h/dt|_{t\rightarrow 0}$ were retained to determine the average $dD_h/dt|_{t\rightarrow 0}$.

Finally, the Cit-AuNPs required a combination of the two approaches, as one of the replicate measurements saw a near-instantaneous increase in D_h while the other did not. In both cases, the calculated $dD_h/dt|_{t\rightarrow 0}$ were not statistically different than zero (*t*-test(116) = 1.37, $p = 0.17$ and *t*-test(9) = 0.62, $p = 0.55$).

The calculated $dD_h/dt|_{t\rightarrow 0}$ for each model ENP are reported in Table S13.

Table S13. Initial aggregation rates ($dD_h/dt|_{t\to 0}$) of model ENPs in filtered WRW.

Surface Coating	Average $dD_h/dt|_{t\to 0}$ (nm/s)
PEG-COOH	0.004 ± 0.005
PEG	-0.015 ± 0.008
PEG-Amine	0.285 ± 0.008*
bPEI	1.104 ± 0.180*
Cit	0.063 ± 0.080

Error bars indicate ± one standard deviation (n = 2).
* Indicates average $dD_h/dt|_{t\to 0}$ is statistically different than zero.

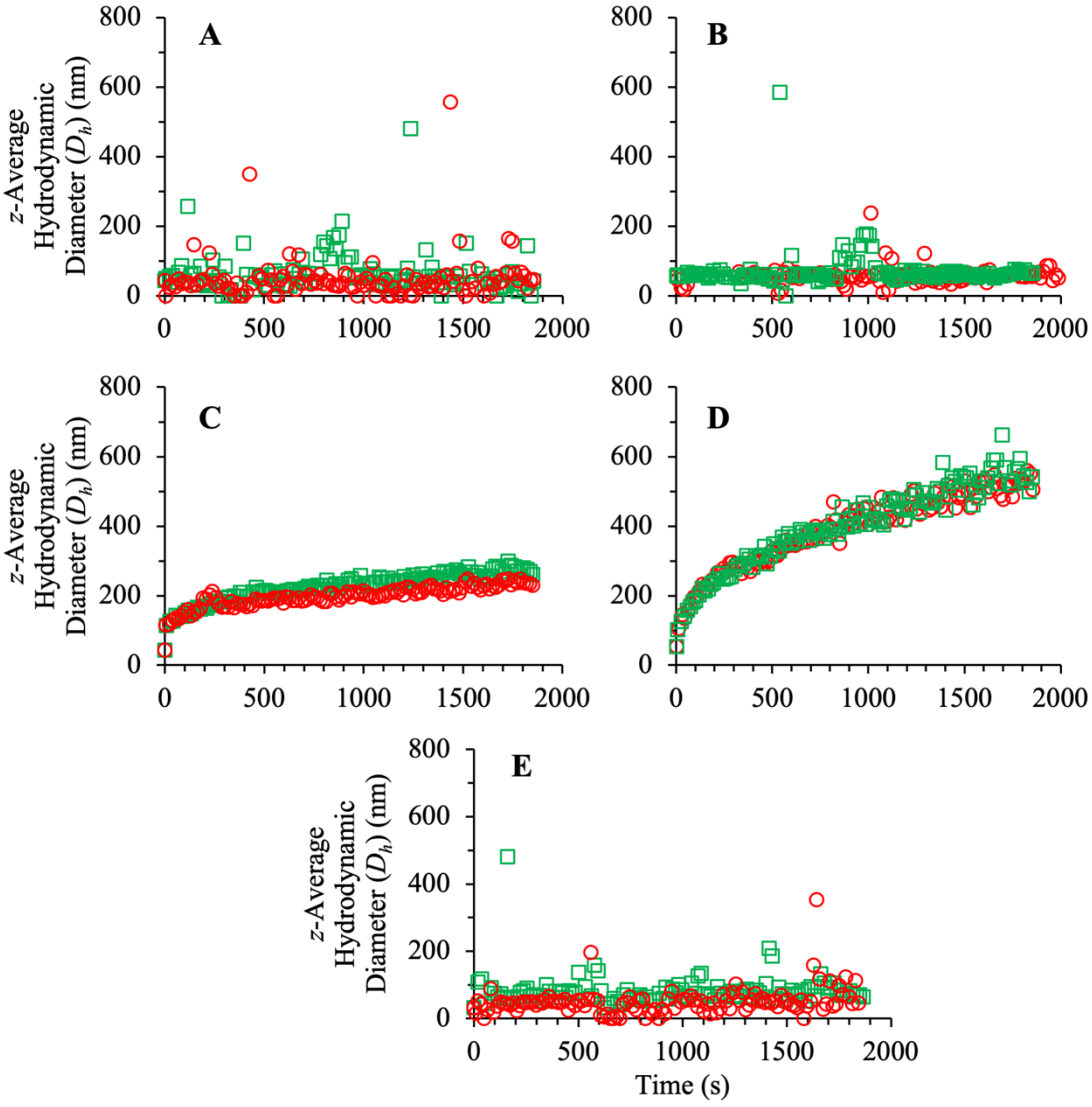

Figure S4. *Z*-average hydrodynamic diameter (D_h) as a function of time for (a) PEG; (b) PEG-COOH; (c) PEG-Amine; (d) bPEI; and (e) Cit-AuNPs dispersed in filtered WRW.

Modelling of Collision Frequency Functions

In the Rectilinear Model detailed by Benjamin & Lawler (2013), the initial collision frequency between two dissimilar particle types (i.e., heteroaggregation of an ENP with a natural colloid [NC]) can be determined by evaluating the mechanisms producing collisions between them. These mechanisms include Brownian motion (${}^{BR}\beta_{NP\text{-}NC}$), differential sedimentation (${}^{DS}\beta_{NP\text{-}NC}$), and fluid shear (${}^{SH}\beta_{NP\text{-}NC}$). Each of these is determined according to Equations 6 – 8 below:

$$ {}^{BR}\beta_{NP-NC} = \frac{2k_BT}{3\mu}\left[\left(\frac{1}{d_{NP}} + \frac{1}{d_{NC}}\right)(d_{NP} + d_{NC})\right] \quad (6) $$

$$ {}^{DS}\beta_{NP-NC} = \frac{\pi}{4}|v_{NP} - v_{NC}|(d_{NP} + d_{NC})^3 \quad (7) $$

$$ {}^{SH}\beta_{NP-NC} = \frac{G}{6}(d_{NP} + d_{NC})^3 \quad (8) $$

Where:

$$ v_{NP,NC} = \frac{g(\rho_{NP,NC} - \rho_w)(d_{NP,NC})^2}{18\mu} \quad (9) $$

When the colliding particles are the same type (i.e., homoaggregation of two ENPs), Equations 6 – 8 simplify to:

$$ {}^{BR}\beta_{NP-NP} = \frac{8k_BT}{3\mu} \quad (10) $$

$$ {}^{SH}\beta_{NP-NP} = \frac{4G}{3}(d_{NP})^3 \quad (11) $$

Where ${}^{DS}\beta_{NP\text{-}NP} = 0$, as two particles with the same characteristics (e.g., ρ_{NP} and d_{NP}) will have the same settling rates and will not undergo collisions due to differential sedimentation.

Using the inputs shown in Table S14, the collision frequency function for each transport mechanism (i.e., ${}^{BR}\beta$, ${}^{DS}\beta$, and ${}^{SH}\beta$) and type of particle interaction (i.e., homo- and heteroaggregation) were modelled. For ENP-NC interactions (heteroaggregation), the collision frequency functions were modelled by varying d_{NC} from 1 – 10^4 nm while fixing d_{NP} at 15 nm (representative of the core diameter measured for the model ENPs). For ENP-ENP interactions (homoaggregation), the collision frequency functions were simplified as only one particle size was necessary to consider (i.e., d_{NP}).

The replicate Coulter Counter measurements performed on the raw WRW indicate an approximate median NC diameter (d_{NC}) of 1.34 ± 0.8 µm (Figure S1). However, considering the size detection limits of the Coulter Counter ($d_{NC} \geq 0.746$ µm) and the trend in the PSD indicating the number

frequency rapidly increases as d_{NC} decreases, it is expected that the 'true' median value of d_{NC} in the raw WRW is well below the instrument detection limits. This expectation is supported by previous research indicating that the majority of NCs (on a number-weighted basis) will have diameters ≪1 µm.[11,12] Regardless, for ENP-ENP and ENP-NC interactions with $d_{NC} \leq 5$ µm, Brownian motion ($^{BR}\beta$) is the dominant collision mechanism owing to the small size of the model ENPs (Figure S5).

Table S14. Inputs used to calculate β for each transport mechanism.

Parameter	Value	Units	Source
Boltzmann Constant (k_B)	1.38 $x10^{-16}$	g cm^2/ s^2 K	Constant
Standard Gravity (g)	9.81	m/s^2	Constant
Density of NC (ρ_{NC})	2.65	g/cm^3	Assumed – SiO_2
Density of AuNP (ρ_{NP})	19.3	g/cm^3	Assumed – Au
Diameter of NC (d_{NC})	1 – 10^4	nm	Assumed
Diameter of AuNP (d_{NP})	15	nm	Measured (TEM)
NC Mass Conc. (C_{NC})	3.9	mg/L	Measured
NP Mass Conc. (C_{NP})	500	µg/L	Measured
Temperature (T)	298	K	Measured
Medium Dynamic Viscosity (μ)	0.0089	g/cm-s	Known – H_2O
Medium Density (ρ_w)	0.997	g/cm^3	Known – H_2O
Time-Averaged Shear Rate (G)	15.6	s^{-1}	Calculated

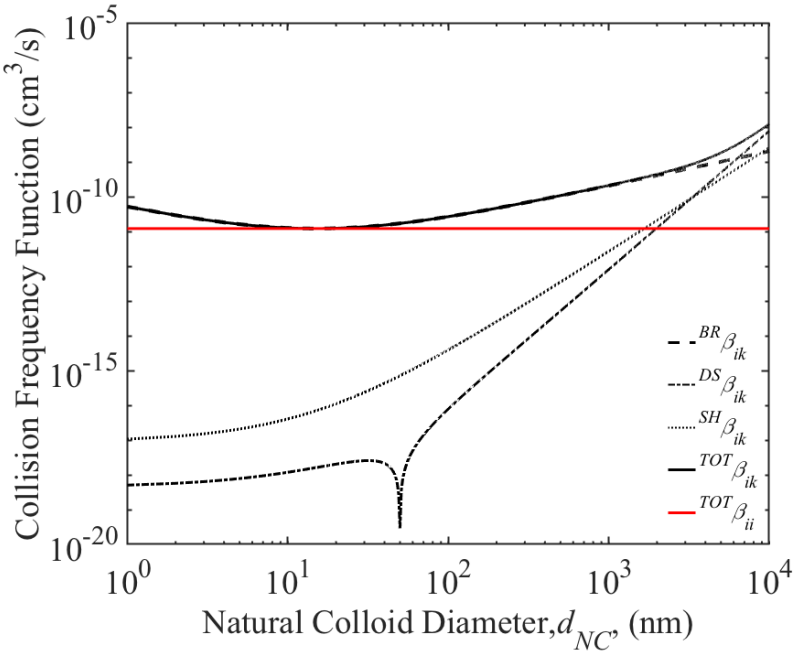

Figure S5. Collision frequency function for each transport mechanism during heteroaggregation ($\beta_{NP\text{-}NC}$) and the total collision frequency function during (solid black) heteroaggregation ($^{TOT}\beta_{NP\text{-}NC}$) and (red) homoaggregation ($^{TOT}\beta_{NP\text{-}NP}$).

Modelling of Initial Aggregation Rates

Initial aggregation rates describing the loss of ENPs via aggregation were modelled using the Smoluchowski Aggregation Equation (Equation 12). For a detailed discussion regarding this equation, the reader is referred to Benjamin and Lawler (2013).

$$\frac{dN_k}{dt} = \frac{1}{2}\alpha_{emp}\sum_{\substack{\text{all i and j}\\ \text{such that}\\ V_i+V_j=V_k}} {}^{TOT}(\alpha_{ij}\beta_{ij})N_iN_j - \alpha_{emp}N_k\sum_{\text{all i}} {}^{TOT}(\alpha_{ik}\beta_{ik})N_i \quad (12)$$

Using Equation 12, the initial rate of change in the number concentration of unaggregated ENPs ($dN_{NP}/dt|_{t\to 0}$) can be modelled. This is accomplished by assuming that ENPs are not formed within the system (i.e., the first set of terms on the right-hand side of Equation 12 is negligible), only collisions from Brownian motion (${}^{BR}\beta$) need to be considered since the other transport mechanisms were found to be negligible within the expected range of d_{NC} (Figure S5), and short-range correction factors (Curvilinear Model) for Brownian motion (${}^{BR}\alpha$) were included to account for the forces arising as two particles approach one another closely.

From this, Equation 12 can be used to describe the loss of ENPs via homoaggregation with other ENPs or via heteroaggregation with the NCs in the system. The former process is realized by recognizing that at early times (i.e., $t \to 0$) the ENPs are represented by a single particle size-class, hence $N_i = N_k = N_{NP}$ with $d_i = d_{NP}$ (fixed at 15 nm). The latter process is realized by assuming that all the NCs are represented by a single particle size-class, resulting in two particle size-classes in the system at early times, i.e., $N_i = N_{NC}$ with $d_i = d_{NC}$ (varying from 0.01 – 1 μm) and $N_k = N_{NP}$ with $d_k = d_{NP}$ (fixed at 15 nm).

$$\left(\frac{dN_{NP}}{dt}|_{t\to 0}\right)_{homo} = -\alpha_{homo}\,{}^{BR}(\alpha\beta)_{NP-NP}N_{NP}^2 \quad (13)$$

$$\left(\frac{dN_{NP}}{dt}|_{t\to 0}\right)_{hetero} = -\alpha_{hetero}\,{}^{BR}(\alpha\beta)_{NP-NC}N_{NP}N_{NC} \quad (14)$$

The relative importance of either mechanism can then be assessed across a range of values for α_{hetero} and α_{homo}, as presented in Figure 3 in the main text.

Characteristic Time for Homo- and Heteroaggregation

Using the modelled initial aggregation rates ($dN_{NP}/dt|_{t\to 0}$) for homo- and heteroaggregation, the characteristic time for the loss of the model ENPs via homo- and heteroaggregation ($t_{char,homo}$ and $t_{char,hetero}$, respectively) can be calculated according to Equations 15 and 16:

$$t_{char,homo} = \frac{N_{NP}}{-\left(\frac{dN_{NP}}{dt}|_{t\to 0}\right)_{homo}} = \frac{1}{\alpha_{homo}{}^{BR}(\alpha\beta)_{NP-NP}N_{NP}} \quad (15)$$

$$t_{char,hetero} = \frac{N_{NP}}{-\left(\frac{dN_{NP}}{dt}|_{t\to 0}\right)_{hetero}} = \frac{1}{\alpha_{hetero}{}^{BR}(\alpha\beta)_{NP-NC}N_{NC}} \quad (16)$$

Using the same inputs presented in Table S14 and discussed in the previous sections, $t_{char,homo}$ and $t_{char,hetero}$ were calculated across a range of d_{NC} and for various values of α_{homo} and α_{hetero}. The results are shown in Figure S6.

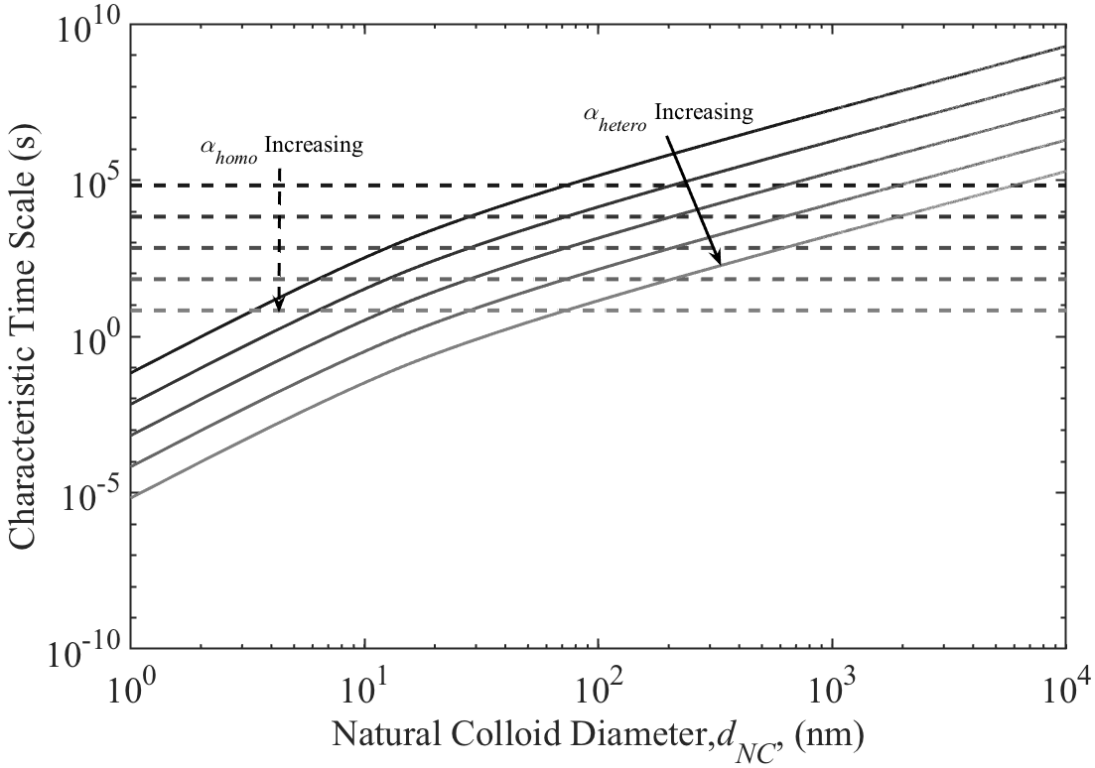

Figure S6. Characteristic time (τ) for (dashed) homoaggregation and (solid) heteroaggregation as a function of d_{NC}, with α_{homo} and α_{hetero} varying between [10^{-4} – 10^{0}].

References

(1) Surette, M. C.; Nason, J. A. Effects of surface coating character and interactions with natural organic matter on the colloidal stability of gold nanoparticles. *Environ. Sci. Nano* 2016, ***3*** **(5)**, 1144–1152.

(2) Henry, D. C. The cataphoresis of suspended particles. Part I. – The equation of cataphoresis. *Proc. Roy. Soc. A* 1931, ***133*** **(821)**, 106.

(3) Ohshima, H. A simple expression for Henry's function for the retardation effect in electrophoresis of spherical colloidal particles. *J. Colloid Interface Sci.* 1994, ***11*** **(1)**, 269 – 271.

(4) Hunter, R.J. *Foundations of Colloid Science, 2nd Edition* 2002. Oxford University Press, London, United Kingdom.

(5) Benjamin, M. M.; Lawler, D.F. *Water Quality Engineering – Physical/Chemical Treatment Processes* 2013. John Wily & Sons, Inc., Hoboken, New Jersey.

(6) American Water Works Association (AWWA) *Standard Methods for the Examination of Water and Wastewater, 22nd Edition* 2012. American Public Health Association.

(7) Karanfil, T.; Erdogan, I.; Schlautman, M. A. Selecting filter membranes DOC and SUVA254. *J. Am. Water Work. Assoc.* 2003, ***95*** (3), 86–100.

(8) Croughan, M. S.; Hamel, J.-F.; Wang, D. I. C. Hydrodynamic effects on animal cells grown in microcarrier cultures. *Biotechnol. Bioeng.* 1987, ***29*** (1), 130–141.

(9) M. Sadowska, Z. Adamczyk, and M. Nattich-Rak, Mechanism of nanoparticle deposition on polystyrene latex particles, *Langmuir*, 2014, **30**, 692-699.

(10) Chen, K. L.; Smith, B. A.; Ball, W. P.; Fairbrother, D. H. Assessing the colloidal properties of engineered nanoparticles in water: case studies from fullerene C 60 nanoparticles and carbon nanotubes. *Environ. Chem.* 2010, ***7*** **(1)**, 10.

(11) Baalousha, M.; Von der Kammer, F.; Motelica-Heino, M.; Baborowski, M.; Hofmeister, C.; Le Coustumer, P. Size-Based Speciation of Natural Colloidal Particles by Flow Field Flow Fractionation, Inductively Coupled Plasma-Mass Spectroscopy, and Transmission Electron Microscopy/X-ray Energy Dispersive Spectroscopy: Colloids−Trace Element Interaction. *Environ. Sci. Technol.* 2006, ***40*** **(7)**, 2156–2162.

(12) Baalousha, M.; von der Kammer, F.; Motelica-Heino, M.; Hilal, H. S.; Le Coustumer, P. Size fractionation and characterization of natural colloids by flow-field flow fractionation coupled to multi-angle laser light scattering. *J. Chromatogr. A* 2006, ***1104*** **(1–2)**, 272–281.